INSTRUMENTATION FOR PROCESS MODELING AND VALIDATION

Analysis and Optimization of Carburizing–Quenching Distortion on Locomotive Gear Ring

XIN WANG [1,2] DAQING LI,[1] and PENG LI[1]

1.—Mechanical Engineering College, Henan University of Engineering, Zhengzhou 451191, China.
2.—e-mail: haiyang630@163.com

The carburizing–quenching distortion (CQD) of the gear ring is difficult to control, considering the heat transfer, phase transformation, and stress effects, so a numerical simulation model of the CQD on the locomotive gear ring was built by DEFORM. The characteristics of the carburized layer and phase transformation of the gear during carburizing–quenching were analyzed, and the deformation mechanism and law on the teeth were analyzed based on the carburized layer and phase transformation results. In order to achieve accurate quantitative analysis, the influence degree and trend of the main process parameters on the CQD were analyzed by an orthogonal experiment aimed at the changes of the addendum circle diameter (ACD) and the common normal length (CNL), and the process parameters were optimized and applied to the production practice. The correctness of the model has been verified by the experimental results, and by comparison with the minimum distortion of the specified process; the expansion of the ACD was reduced by 29.8%, and the expansion of the CNL was reduced by 32.7% under the optimal process parameters.

INTRODUCTION

Locomotive gear operates at high speeds and requires reliable and stable operation under severe cold, high temperature, and tunnel environments, so higher requirements are placed on the long-life, anti-fatigue and high-strength design and manufacturing technology of gears. Carburizing–quenching has become the main surface heat-treatment process of high-parameter hardened gears, because it can make the surface of the gears have a higher hardness and can simultaneously guarantee the toughness of the core.[1,2] It also plays a crucial role in improving the wear resistance, plastic deformation resistance, surface contact fatigue resistance, and bending fatigue resistance of gears. However, the carburizing–quenching process is complicated, and there are many influencing factors of the material and the process. The surface and core of the gear have high temperatures, microstructures, and stress differences, which cause the gear to be easily distorted. Larger distortion leads to an increase in production costs on gear grinding, and a reduction in the manufacturing precision and load-carrying capacity of the gears. Therefore, the distortion control of carburizing–quenching on locomotive gears has become one of the prominent technical difficulties. The distortion of the gears during the carburizing–quenching process is closely related to the internal heat transfer, phase transformation, and internal stress. The traditional solution to the distortion is to rely on practical experience, which basically does not produce accurate control, and takes a lot of manpower and material resources, so it can no longer meet the high-precision requirements of current industrial production. The finite element method simulation on carburizing–quenching has been used to simulate the temperature, phase transformation, and stress results. Many results that cannot be extracted by traditional experiments and experience can be obtained by the simulation. It provides an effective way to clearly reveal the law of distortion and to control the distortion, so it has become the current frontier in the international heat-treatment field.[3,4]

Sugimoto et al.[5] used the finite element method to simulate the gas-quenching process of the carburizing helical bevel gear, and analyzed the influence of the gas pressure, gas flow rate, and cooling rate on gear distortion. Sugianto et al.[6] measured the heat transfer coefficient at different positions of the helical gears, analyzed the quenching process of them by finite element software, and simulated the changes on the microstructure transformation, deformation, and residual stress. In combination with the thermal and mechanical properties with temperature variations calculated by JMAT-Pro, Pang et al.[7] compared the deformation of solid and hollow gear shafts by simulation and practice. The results showed that the deformation of hollow shafts was much smaller than that of solid ones, and that the overall quality of the shafts was improved. Khan et al.[8] focused on the development of an integrated modeling scheme of a carburizing–quenching–tempering process using chemical composition-dependent, microstructure-based models for gear manufacturing. The utility of the model has been proved by the production of a typical gear. O'Brien et al.[9] simulated the effect of carburization and different retained austenite contents on macroscale fatigue behavior of spur gear by the finite element method. The results showed that the carburized case with high retained austenite gives rise to a better fatigue life compared to that with low retained austenite. Li et al.[10] simulated the carburizing–quenching process of helical gears. The model predicted the distortion mechanism of gear during carburizing–quenching, and provided a reliable basis. Lee et al.[11] predicted the variations in microstructure and deformation occurring during carburizing–quenching processes of a SCM420H gear by the finite element method, and the simulated results were well verified with experimental data. The above studies have mostly focused on how to accurately simulate carburizing–quenching processes and the distortion rule. However, there are few studies on the impact trends and degrees of the carburizing–quenching process parameters on the gear distortion, and few studies have achieved precise control of the carburizing–quenching distortion by optimization of the process parameters. In this study, by the coupling of the temperature, transformation, and stress fields, firstly, a corresponding carburizing–quenching analysis model was built on a locomotive gear ring, and the mechanism of tooth distortion was explained by the analysis results, then, secondly, the influence of the process parameters on the gear distortion was accurately analyzed by an orthogonal experiment. The optimal process parameters were applied to the production practice and a good distortion control effect was obtained.

EXPERIMENT MODEL AND METHOD

Gear Structure and Model

The structure of the gear is shown in Fig. 1. The outer diameter of the gear is nearly 1 m, and the thickness of the gear is relatively thin. The material of gear ring is made of 17CrNiMo6 steel, and the chemical composition is Fe-0.17C-0.27Si-0.65Mn–1.61Cr-0.29Mo-1.57Ni (wt.%). For the sake of the calculations and to save time, a single-tooth model with the tetrahedral mesh was built for analysis by DEFORM, as shown in Fig. 1. In the model, symmetrical constraints were imposed on both sides, and considering that the gear is laid flat in the furnace, a fixed constraint has been implemented on the end of the gear.

Experiment Method

The carburizing–quenching process of the gear is shown in Fig. 2. The process parameters, such as carburizing temperature (CT), boost carbon potential (BCP), boost carburizing time (BCT), quenching temperature (QT), quenching holding time (QHT), oil temperature (OT), and oil quenching time (OQT) were selected for analysis. Each process parameter was set based on the material characteristic and production practice. The carbon potential in the diffusion was set to 0.78%. Each process parameter was designed at three levels, and orthogonal tests with 3 levels and 7 factors were performed in 18 simulation experiments (L18 (3^7)), as shown in Table I. Based on the characteristics of the finite element analysis, the changes of the ACD and CNL were selected as the distortion indicators to determine the influence of the process parameters on the gear distortion. The ACD change mainly affects the amount of grinding teeth in the later period and the radial matching accuracy of the gear pair. The CNL change mainly affects the post-gear-machining precision and the side matching accuracy of the gear pair.

NUMERICAL SIMULATION EQUATION

Carburizing Equation

Fick's diffusion law is widely used in the carburizing calculation:[12]

$$\frac{\partial C}{\partial t} = D\frac{\partial^2 C}{\partial x^2} \tag{1}$$

$$\text{Initial condition}: \quad C(x,0) = C_0 \tag{2}$$

The third boundary condition :
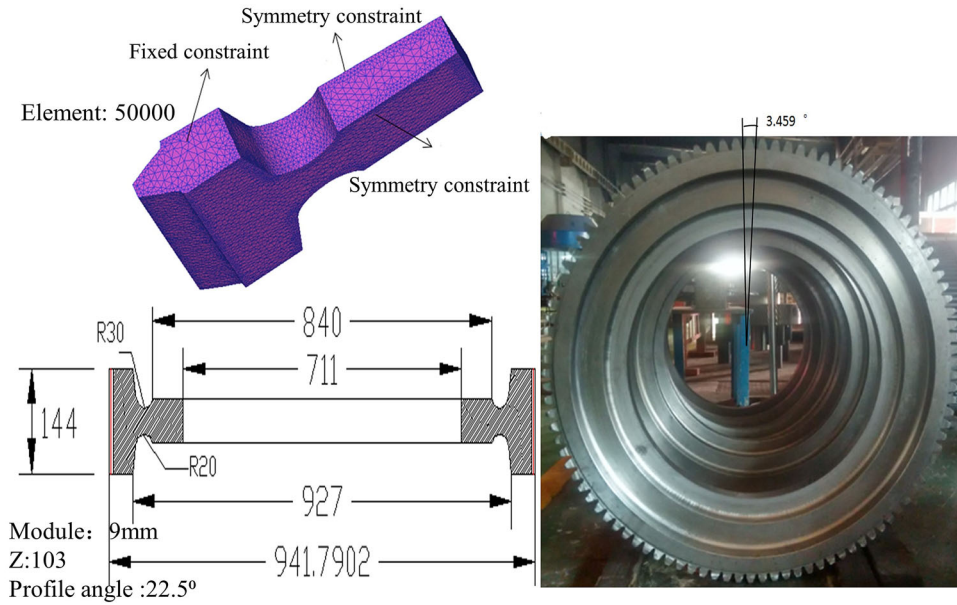$$D\left(\frac{\partial C}{\partial x}\right) = \beta(C_s - C_\rho) \tag{3}$$

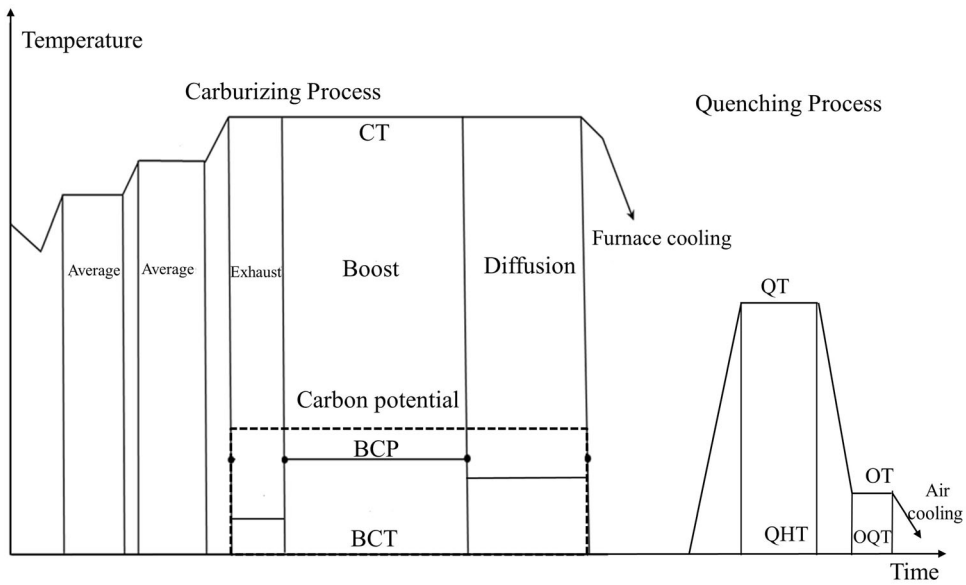Fig. 1. The structure and model of the gear.

Fig. 2. Carburizing–quenching process.

Table I. Process parameters and level

	CT (°C)	QT (°C)	BCT (h)	BCP (%)	OT (°C)	OQT (s)	QHT (s)
Level 1	910	810	15	1.1	40	1800	9000
Level 2	920	825	17	1.2	60	3600	10,800
Level 3	930	840	19	1.3	80	5400	12,600

where t and x indicate time and the position direction, respectively, C_0, C_s, and C_ρ denote original carbon content, carbon content on the surface and carbon potential, respectively,

D is the diffusion coefficient, and β is the carbon transfer coefficient. Based on the conclusion of Zhang,[13] $\beta = 0.0001123$ mm/s. Kim et al.[14] proposed a diffusion coefficient equation depending on the temperature and carbon content. The role of alloying elements was also considered in this paper, as:

$$D(T, C) = \left(0.0047 \exp(-1.6C) \exp\left[\frac{-(37000 - 6600C)}{RT} \right] \right) \times q$$

(4)

where T and C denote the temperature and carbon content, respectively, and q is the coefficient of alloying elements, which can be determined by the following empirical equation:[15]

$$q = 1 + (0.15 + 0.033\text{Si})\text{Si} - 0.0365\text{Mn} \\ - (0.13 - 0.0055\text{Cr})\text{Cr} + (0.03 - 0.03365\text{Ni})\text{Ni} \\ - (0.025 - 0.01\text{Mo})\text{Mo}$$

(5)

Temperature Field and Phase Transformation Analysis

The temperature field is based on a conduction equation considering the latent heat of phase transformation:[16]

$$\rho c \dot{T} - \frac{\partial}{\partial \chi_i} \left(k \frac{\partial T}{\partial \chi_i} \right) + \sum \rho_i \iota_i \dot{\xi} = 0$$

(6)

where $\rho, c,$ and k are the density, the specific heat, and the heat conductivity, respectively, and ι_i is the latent heat due to the progressive phase, i. The latent heats of ferrite, pearlite, bainite, and martensite transformation are 590 J/mm^3, 600 J/mm^3, 620 J/mm^3, and 640 J/mm^3, respectively.[13]

The thermal convection boundary condition is the boundary condition of heat transfer:[17]

$$-k \frac{\partial T}{\partial \chi_i} n_i = h(T_s - T_f)$$

(7)

where n_i denotes the boundary scope of the workpiece, T_s and T_f denote the surface temperature and the oil temperature, respectively, and h denotes the heat transfer coefficient of the quenching oil, which was set based on the literature.[6]

The martensite transformation considers the effects of the temperature and carbon content in Eq. 9:[18]

$$\xi_M = 1 - \exp(\psi_1 T + \psi_2(C - C_0) + \phi_4)$$

(9)

where ξ_M is the volume fraction of martensite, C_0 is the initial carbon content ($C_0 = 0.17$), ψ_1 and ψ_2 are, respectively, the coefficient of the temperature and carbon content, and φ_4 is the constant coefficient. The martensite transformation temperature (M_S) and martensite transformation temperature when martensite content is 50% (M_{50}) of 17CrNiMo6 steel with the initial carbon content are 375.7°C and 341.7°C, respectively. So, ψ_1 and φ_4 are 0.020395 and -7.6848, respectively. When the carbon content is 0.8%, M_S was calculated based on the conclusions of Lee and Park,[19] as:

$$M_S = 475.9 - 335.1\text{C} - (34.5\text{Mn} + 1.3\text{Si} + 15.5\text{Ni} \\ + 13.1\text{Cr} + 10.7\text{Mo} + 9.6\text{Cu}) + 11.67 \ln(d_r)$$

(10)

where each element symbol represents the mass percentage of the alloy element, and d_r represents the average diameter of the austenite grain, and is set to 30 μm. So, when the carbon content is 0.8%, $M_s = 176.2$°C. Substitute M_s into Eq. 10 and recalculate $\psi_2 = 6.494$.

Distortion Equation

The total strain rate is assumed to be divided into elastic ($d\varepsilon_{ij}^E$), plastic ($d\varepsilon_{ij}^p$), thermal ($d\varepsilon_{ij}^{th}$), phase transformation ($d\varepsilon_{ij}^{tr}$), and phase transformation plasticity ($d\varepsilon_{ij}^{tp}$) strain rate according to Eq. 11. Each strain rate is calculated as shown in Eqs. 12–16:[20,21]

$$d\varepsilon = d\varepsilon_{ij}^E + d\varepsilon_{ij}^p + d\varepsilon_{ij}^{th} + d\varepsilon_{ij}^{tr} + d\varepsilon_{ij}^{tp}$$

(11)

$$d\varepsilon_{ij}^E = \frac{1}{2G} d\sigma_{ij}$$

(12)

$$d\varepsilon_{ij}^p = \frac{3}{2H} \frac{d\sigma_i}{\sigma_i} \sigma_{ij}$$

(13)

$$d\varepsilon_{ij}^{th} = \sum_{k=1}^{5} m_i \alpha_i(T) dT$$

(14)

$$d\varepsilon_{ij}^{tr} = \sum_{k=2}^{5} dm_i \beta_i^T$$

(15)

$$d\varepsilon_{ij}^{tp} = 3K\sigma_{ij}(1 - m_i)\Delta m_i$$

(16)

In Eqs. 12–16, G is the shear modulus, H is the strain hardening index, m_i and α_i are the volume fraction and expansion coefficient of the microstructure, respectively, β_i^T is the coefficient of the phase

transformation, which is related to the temperature and carbon content, And K is the transformation plasticity coefficient (I = 1, 2, 3, 4, and 5 representing austenite, ferrite, pearlite, bainite, and martensite, respectively). The changes of thermal and physical property parameters with the temperature and carbon content (C) are shown in Table II and Fig. 3.

RESULTS AND DISCUSSION

The Carburizing–Quenching Results

The specified analysis results indicate the characteristics of the carburizing, phase transformation, and distortion of the gear. The specified process parameters are: CT is 920°C, BCP is 1.2%, BCT is 17 h, QT is 820°C, QHT is 6 h, OT is 60°C, and OQT is 3600 s. The carbon content of the furnace sample was determined by an X-350A spectrometer, and the measured surface carbon content was 0.79%. Figure 4 shows the distribution of carbon content after carburizing in the middle of the tooth width. The maximum carbon content of the gear ring was 0.8%, which is basically consistent with the measured result. Due to the different convex and concave structures of the gear, the carbon content near the addendum is obviously higher than that of the other position.

Figure 5a shows the results of the martensite and retained austenite in the sectioned half tooth during oil-quenching. Most of the tooth has transformed into the martensite. The martensite content was up

to 97.5%, mainly distributed in the core of the tooth. The retained austenite content of points P1 and P2 was 12% and 9%, respectively. There was almost no retained austenite at point P3. The martensite change of the three tracking points during oil-quenching is shown in Fig. 5b. Point P1 is the surface point at the end of the gear, and points P2 and P3 are the surface and center points in the middle of the tooth width, respectively. The corresponding carbon content of the three points is 0.76%, 0.74%, and 0.22%. Based on Eq. 10, the M_s corresponding to the three points are 210.7°C, 217.4°C and 391.7°C, respectively, the martensite contents of the three points were 84.8%, 83.5%, and 94.7%, respectively, and the times of martensite transformation of the three points were 26 s, 29 s, and 12 s, respectively. The carbon content at point P3 is lower and Ms is higher, so the martensitic transformation at point P3 occurred and completed first. The carbon contents at points P1 and P2 on the surface are higher and Ms is lower, so, even if the cooling rate on the surface is faster than that in the core, the martensite transformation at both points still occurred later. The cooling rate at point P1 was faster than that at point P2, so the martensite transformation occurred slightly earlier than that at point P2, and the martensite content is slightly higher than that of point P2. After being corroded, the surface and core microstructures at the addendum of the tooth shape sample in the furnace were observed by optical microscope, as shown in Fig. 6. The surface microstructure was acicular

Table II. Thermal expansion coefficients of 17CrNiMo6

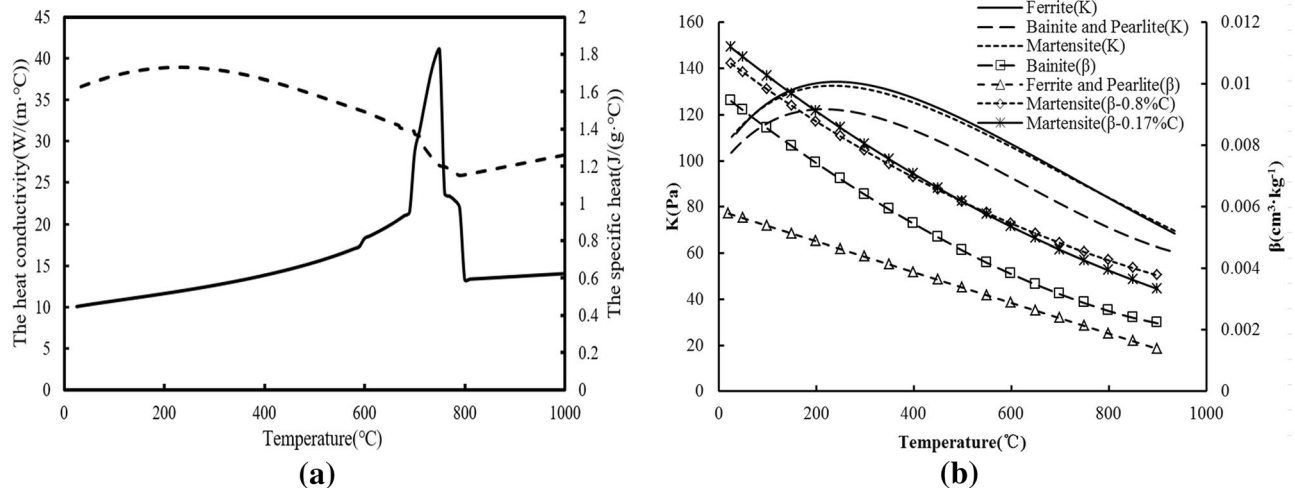| Austenite	Ferrite and pearlite	Bainite	Martensite
2.2×10^{-5} (0.17%C) 1.8×10^{-5} (0.8%C)	1.2×10^{-5}	1.3×10^{-5}	1.1×10^{-5} (0.17%C) 9.8×10^{-6} (0.8%C)

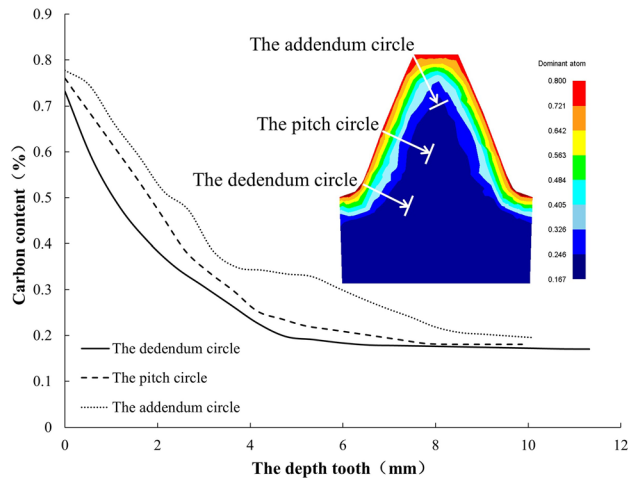Fig. 3. The thermal (a) and physical property (b) parameters of 17CrNiMo6.

Fig. 4. Carbon content distribution result.

martensite, retained austenite, and granular carbide, and the core microstructure was lath martensite and a small amount of free ferrite.

The radial displacement changes at points P1 and P3 during oil-quenching are shown in Fig. 7a. In the first 52 s, due to the small amount of formed martensite, the volume expansion caused by the martensite transformation was very small, the radial displacement was mainly affected by the volume contraction caused by oil-cooling, and so the radial displacement decreased rapidly from initial expansion to contraction deformation. By comparison with point P3, point P1 had a faster cooling speed, so its displacement decreased the most. Then, when the time was 142 s, the martensite transformation at both points was basically completed, the volume expansion caused by martensite transformation resisting the volume contraction caused by °C oil-cooling. Finally, the radial expansion caused by the transformation was larger than the radial contraction caused by °C oil-cooling, so the radial displacement at both points showed a slight expansion. By comparison with point P1, the martensite transformation at point P3 occurred first, a large number of high-strength martensite was generated, and the retained austenite was less at point P3. The thermal expansion coefficient of austenite was the largest in the microstructure, while less austenite promoted the radial expansion during oil-quenching, so its radial displacement expansion is the larger. The volume expansion caused by the martensite transformation at point P1 was blocked by the martensite in the core, and the retained austenite was more, so the final radial expansion was smaller than that at point P3.

Figure 7b shows the radial distortion results of the gear. The maximum displacement was 1.02 mm and appeared on the wheel hub. Except for a slight contraction near both ends, the gear tooth presents the expansion deformation along the tooth width. That is, along the tooth width direction, the gear
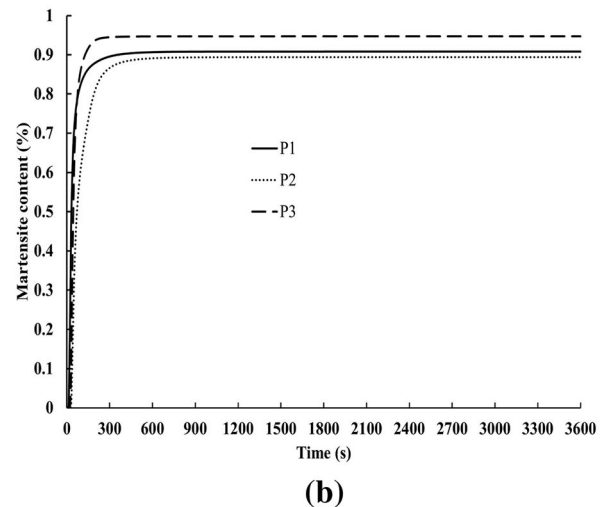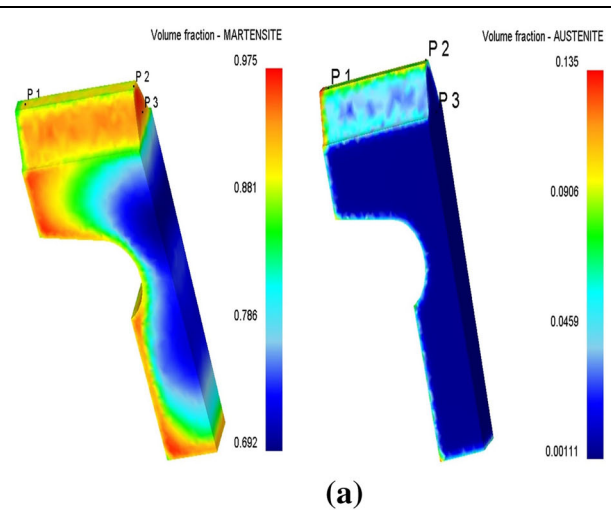

Fig. 5. Phase transformation result in the sectioned half tooth (a) and martensite change curve (b).

tooth presents a lumbar drum-shaped deformation. The curve in Fig. 7b shows a radial drum-shaped deformation in the tooth width direction. In the middle of the tooth width the displacement is the maximum, which is 0.325 mm, so the ACD is expanded by 0.65 mm under this process. In the tooth width direction in Fig. 7b, the thickness of the teeth had a small expansion, which led to the expansion of the CNL. The measured CNL expansion was 0.47 mm.

Distortion Results in the Orthogonal Experiment

In summary, the changes of the ACD and CNL are mainly caused by the thermal expansion of the gear and volume change of the phase transformation in the carburizing–quenching process. The final distortion result is the mutual equilibrium result
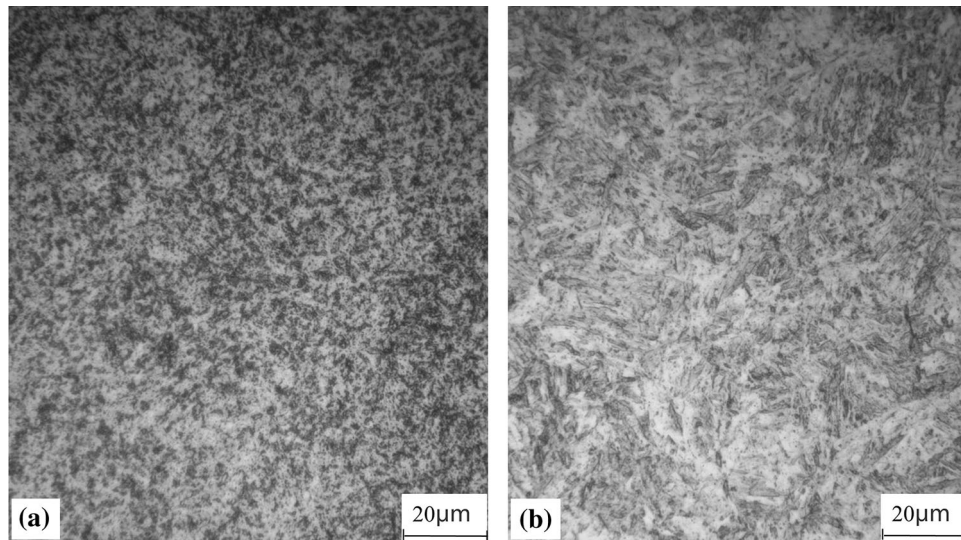
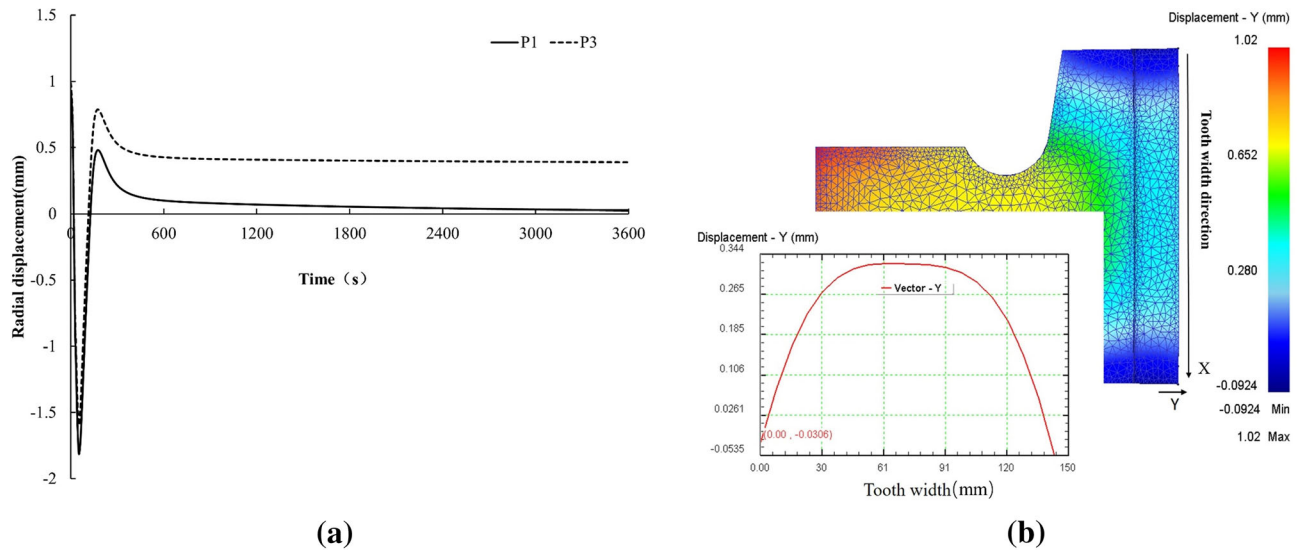Fig. 6. The surface (a) and core (b) microstructures of the tooth shape sample.

Fig. 7. Radial deformation history (a) and result (b).

between the thermal expansion and the volume change of the phase transformation during carburizing–quenching. Based on the results of the orthogonal experiment, the change of the ACD and CNL with every process parameter are shown in Fig. 8. The changes of the ACD and CNL are positive, that is, both indicators have a certain expansion after carburizing–quenching. The change of the ACD is generally higher than the change of the CNL, so the radial distortion is greater than the side distortion on the gear.

The Influence of Process Parameter on Distortion

The higher BCP, the higher carbon content on the surface, which will reduce the thermal expansion coefficient of the austenite and martensite, and the

increase of carbon content will increase the volume change during martensite transformation and microstructure stress, so a high carbon content is bound to increase the distortion. In Fig. 8, it can be seen that, as the BCP increased, both distortions showed an increasing trend. Especially, when the BCP was 1.3%, there was a certain abrupt change in the ACD and CNL. The higher the CT, the faster the carbon diffusion rate in austenite, and the higher the surface carbon content, so both distortions will also increase. However, the increase in the ACD is slower, and the increase in the CNL is greater. The BCT had no obvious rule on both distortions, but when the BCT was 19 h, both distortions were at the minimum.

The higher the QT, the greater the temperature difference between the gear and the oil, so the
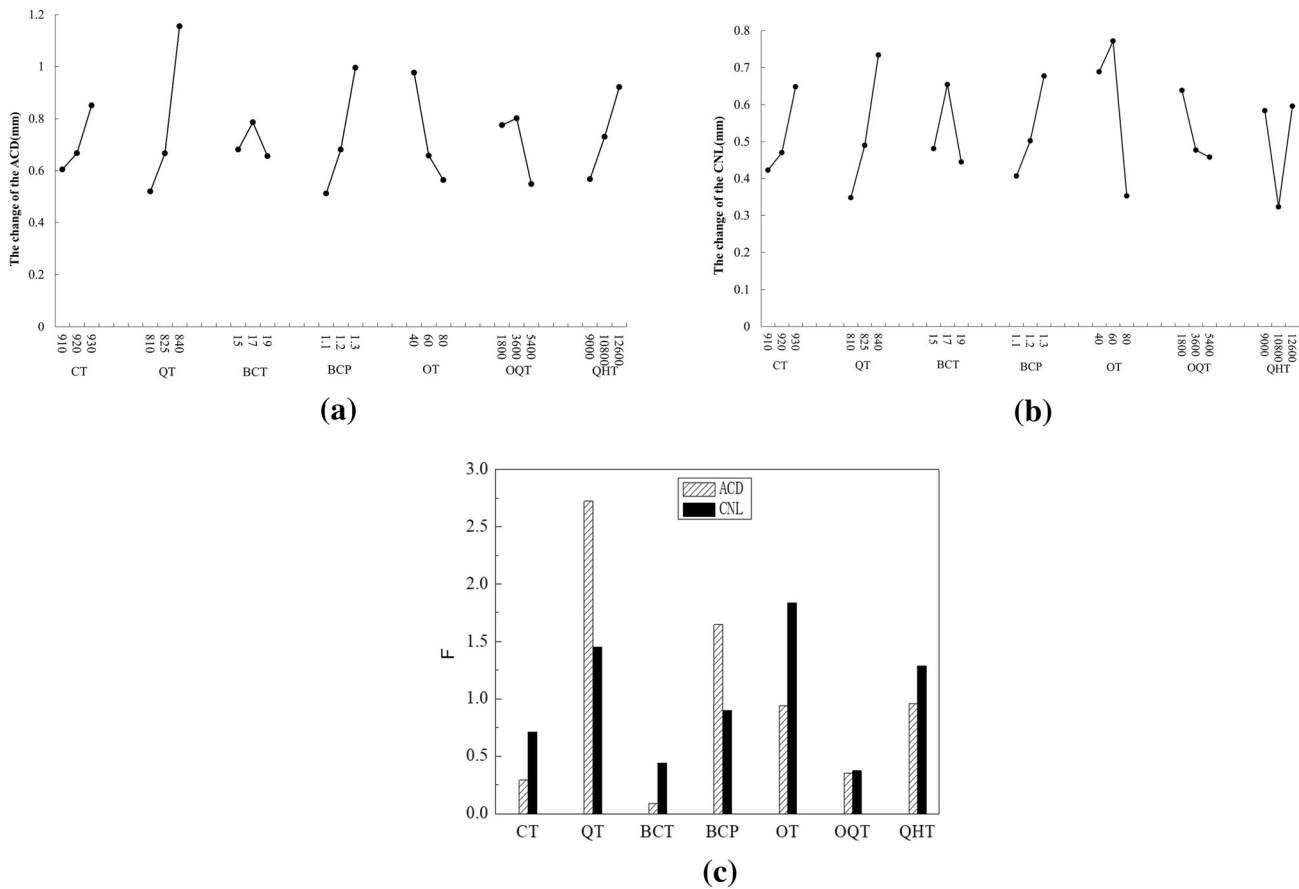
Fig. 8. The influence of various factors on the change of the ACD (a) and CNL (b); F ratio results of all factors (c).

cooling time and contraction become larger in the oil, and the microstructure stress and distortion become larger during martensitic transformation. When the QT increased to 840°C, a large abrupt change occurred in the ACD and CNL, indicating that the QT had a greater influence on both distortions. The larger the size of the gear, the longer the QHT, the smaller the temperature difference between the surface and the core, the greater the austenitizing degree and the grain size, which will increase the microstructure stress and cooling contraction during the quenching, while the residual austenite will also simultaneously be more, resulting in more oxidative decarburization, so the distortion will increase. The distortion of the ACD increased with the increase of the QHT, and the distortion of the CNL was also the largest when the QHT was 12,600 s, but the minimum distortion occurred when the QHT was 10,800 s, so the QT and QHT can be appropriately reduced to reduce the distortion. The higher the OT and the longer the OQT, the smaller the temperature difference between the gear and the oil, the smaller the cooling contraction, the smaller the thermal stress generated, and the lower the martensite transformation during oil-quenching, so the distortion should be smaller. In Fig. 8, when the OT was raised from

40°C to 60°C and the OQT was increased from half an hour to 1 h, the distortion increased slightly in contrast, but, as the OT and OQT increased continuously, both distortions showed a downward trend on the whole.

The Influence Degree of Each Factor and the Optimization Process

According to the variance analysis method of the orthogonal experiment, the F ratio refers to the ratio of the average difference sum of the factors to the mean difference sum of the errors. The larger the F ratio of a certain factor, the greater the influence of that factor on the experimental results. Figure 8c shows the F ratio of each factor. It can be seen that the influence of various factors on the change of the ACD from hard to weak, in turn, is that QT, BCP, QHT, OT, OQT, CT, and BCT, and the influence of various factors on the change of the CNL from hard to weak, in turn, is that of OT, QT, QHT, BCP, CT, BCT, and OQT. Although each factor has a different influence on both distortions, the QT, OT, BCP, and QHT all have a great influence on the distortion.

Considering the influence trend and degree of various factors on both distortions, the optimum process parameters have been determined with the
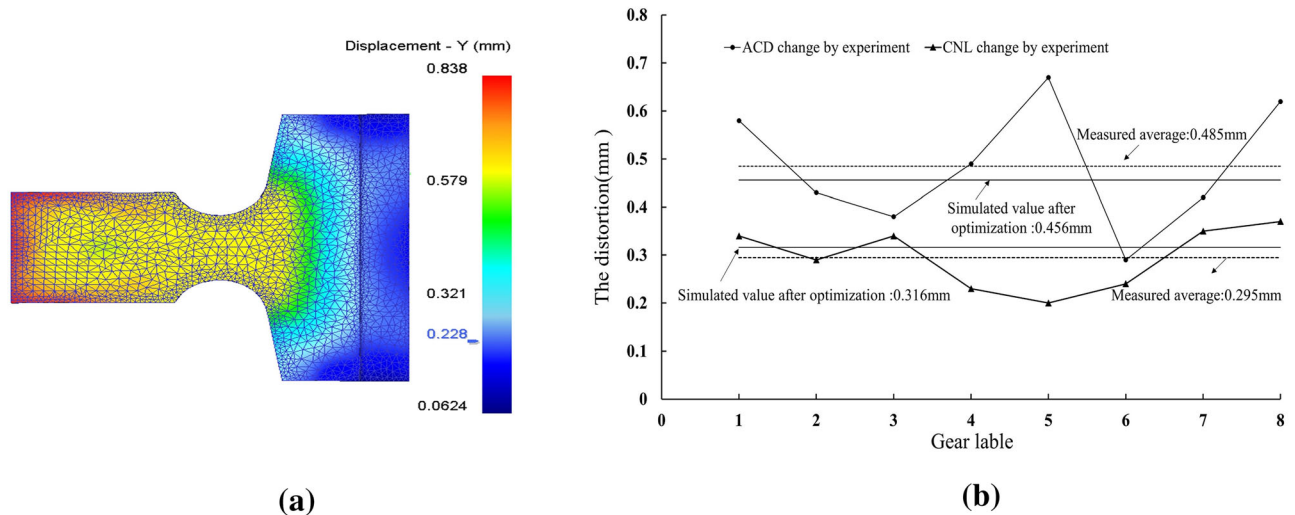
Fig. 9. The simulation (a) and experiment (b) optimal results of gear distortions.

aim of the minimum two distortions. The CT is 910°C, the BCP is 1.1%, the BCT is 19 h, the QT is 810°C, the QHT is 10,800 s, the OT is 60°C, and the OQT is 5400 s in the optimal process. The simulation proceeded under the optimal process parameters, and the optimal distortion result is shown in Fig. 9a. The expansion of the ACD was 0.456 mm, and the expansion of the CNL was 0.316 mm. By comparison with the minimum distortion of the specified process, the expansion of the ACD is reduced by 29.8%, and the expansion of the CNL is reduced by 32.7% under the optimal process parameters.

In order to verify the simulation results, under the same process conditions, the tooth shape sample and 8 gear rings were subjected to furnace testing. The distortion of the ACD and CNL in the middle of the gear width was measured, as shown in Fig. 9b. The simulated value of both distortions was within the range of the measured value: the average expansions of the ACD and CNL was 0.485 mm, and 0.295 mm, respectively, and the differences between the simulated and experiment data on the expansion of the ACD and CNL was 0.029 mm and 0.021 mm, respectively. The simulation results are in good agreement with the experiment results. The hardness gradient distribution at the addendum of the tooth shape sample was measured, as shown in Fig. 10. Based on the standard of the gear, the gear with a depth greater than 52.3 HRC was used as the hardened case, and the hardened case of the sample was about 2.65 mm, and the surface hardness was 59 HRC. The surface hardness and the hardened case of the gear ring all meet the technical requirements under the optimum process conditions, showing that the optimal process parameters determined by the simulation can be applied to the actual production.
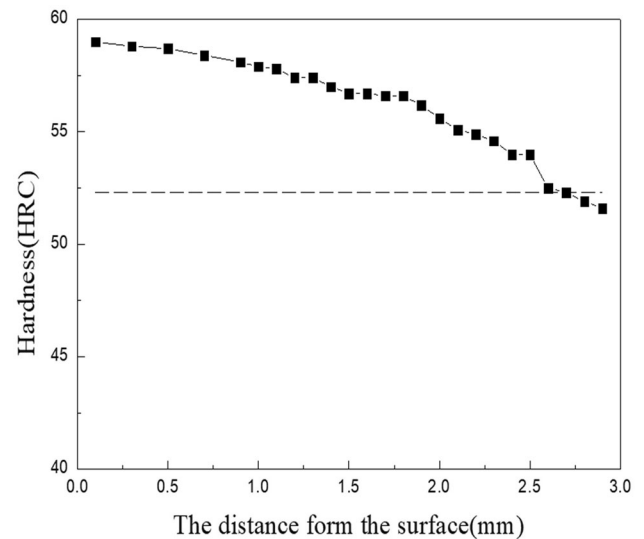

Fig. 10. Hardness gradient of tooth shape sample.

CONCLUSION

(1) Comprehensively considering the temperature, phase transformation, and stress field, an analysis model of carburizing–quenching on the locomotive gear ring was built. In order to improve the accuracy of the analysis, the influence of alloying elements on the diffusion coefficient was considered in the carburizing, and the effect of carbon content on the martensitic transformation was considered during the quenching.

(2) Aimed at the changes of the ACD and CNL, the influence degree and trend of each process factor on both distortions were studied by an orthogonal experiment. By comparison with

other factors, the QT, OT, BCP, and QHT had a greater effect on both distortions.

(3) With the aim of the minimum two distortions, the optimal process parameters were obtained. The QT is 910°C, the BCP is 1.1%, the BCT is 19 h, the QT is 810°C, the QHT is 10,800 s, the OT is 60°C, and the OQT is 5400 s in the optimal process. The furnace test proceeded under the optimal process parameters. It was found that the distortion error between the simulation result and the experimental result was small, and that the simulation results had good accuracy and could guide the actual production. The surface hardness and the hardened case of the gear ring all simultaneously met the technical requirements under the optimum process conditions.

ACKNOWLEDGEMENTS

CONFLICT OF INTEREST

The authors declare that they have no conflict of interest.

REFERENCES

1. J.J. Hu, C.P. Ma, Y. Liu, and F. Sun, *Hot Work. Technol.* 46, 231 (2014).
2. J.G. Chen, *J. Mech. Transm.* 38, 152 (2014).
3. W. Shao, M.H. Yi, J.Y. Tang, and S.Y. Sun, *Chin. J. Mech. Eng.* 35, 2 (2022).
4. Y. Bouissa, N. Bohlooli, D. Shahriari, H. Champliaud, J.B. Morin, and M. Jahazi, *J. Manuf. Process.* 58, 592 (2020).
5. T. Sugimoto, M. Qin, and Y. Watanabe, *B.H.M.* 151, 451 (2006).
6. A. Sugiantoa, M. Narazakib, M. Kogawara, A. Shirayorib, S.Y. Kim, and S. Kubotac, *J. Mater. Process. Technol.* 209, 3597 (2009).
7. Pang, S.J. Yu, and J.W. Xu, *Phys. Procedia* 50, 103 (2013).
8. Khan and B. Gautham, *Integr. Mater. Manuf. Innov.* 7, 28 (2018).
9. E.C.H.C. O'Brien and H.K. Yeddu, *J. Mater. Sci. Technol.* 49, 157 (2020).
10. X.S. Li, D.Y. Ju, J.T. Cao, S.R. Wang, Y. Chen, F.B. He, and H. Li, *Coatings* 11, 1224 (2021).
11. K.H. Lee, J. Han, G.S. Kim, S.D. Yun, and Y.K. Lee, *J. Korean Soc. Heat Treat.* 28, 300 (2015).
12. N.K. Kim and K.Y. Bae, *Int. J. Precis. Eng. Manuf.* 16, 73 (2015).
13. X. Zhang and J.Y. Tang, *Heat Treat. Met.* 40, 185 (2015).
14. D.W. Kim, Y.G. Cho, H.H. Cho, S.H. Kim, W.B. Lee, M.G. Lee, and H.N. Han, *Met. Mater. Int.* 17, 885 (2011).
15. A. Sugianto, M. Narazaki, and M. Kogawara, *J. Mater. Eng. Perform.* 19, 194 (2010).
16. S.H. Kang and Y.T. Im, *J. Mater. Process. Technol.* 192–193, 381 (2007).
17. J.P. Schillé and Z.L. Guo, *Mater. Manuf. Process.* 26, 137 (2011).
18. Y. Liu, S.W. Qin, Q.G. Hao, N.L. Chen, X.W. Zuo, and Y.H. Rong, *Metall. Mater. Trans. A* 48, 1 (2017).
19. S.J. Lee and K.S. Park, *Metall. Mater. Trans. A* 44, 3423 (2013).
20. J. Li, Y. Min, P. Wang, X. Cai, and X. Wu, *Met. Mater. Int.* 25, 546 (2019).
21. B.L. Ferguson, Z. Li, and A.M. Freborg, *Comput. Mater. Sci.* 34, 274 (2005).